Probing the Motional Behavior of Eumelanin and Pheomelanin with Solid-State NMR Spectroscopy: New Insights into the Pigment Properties

ARTICLE *in* CHEMISTRY - A EUROPEAN JOURNAL · AUGUST 2012

Impact Factor: 5.73 · DOI: 10.1002/chem.201200277 · Source: PubMed

7 AUTHORS, INCLUDING:

Fabio Ziarelli
French National Centre for Scientific Resea…
117 PUBLICATIONS **1,254** CITATIONS
SEE PROFILE

Patrick J Farmer
Baylor University
100 PUBLICATIONS **2,689** CITATIONS
SEE PROFILE

Stéphane Viel
Aix-Marseille Université
84 PUBLICATIONS **1,318** CITATIONS
SEE PROFILE

Giulia Mollica
Aix-Marseille Université
30 PUBLICATIONS **372** CITATIONS
SEE PROFILE

CHEMISTRY
A EUROPEAN JOURNAL

FULL PAPER

DOI: 10.1002/chem.201200277

Probing the Motional Behavior of Eumelanin and Pheomelanin with Solid-State NMR Spectroscopy: New Insights into the Pigment Properties

Pierre Thureau,[a] Fabio Ziarelli,[b] André Thévand,[a] Rachel W. Martin,[c] Patrick J. Farmer,[d] Stéphane Viel,[a] and Giulia Mollica*[a]

Abstract: Melanin is the most widespread pigment in the animal kingdom. Despite its importance, its detailed structure and overall molecular architecture remain elusive. Both eumelanin (black) and pheomelanin (red) occur in the human body. These two melanin compounds show very different responses to UV-radiation exposure, which could relate to their microscopic features. Herein, the structural properties and motional behavior of natural eu- and pheomelanin extracted from black and red human hair are investigated by means of solid-state NMR spectroscopy. Several 1D and 2D NMR spectroscopic techniques were combined to highlight the differences between the two forms of the pigment. The quantitative analysis of the ^{1}H NMR wide-line spectra extracted from 2D ^{1}H–^{13}C LG-WISE experiments revealed the presence of two dynamically distinguishable components in both forms. Remarkably, the more mobile fraction of the pigment showed a higher mobility with respect to the proteinaceous components that coexist in the melanosome, which is particularly evident for the red pigment. An explanation of the observed effects takes into account the different architecture of the proteinaceous matrix that constitutes the physical substrate onto which melanin polymerizes within the eu- and pheomelanosomes. Further insight into the molecular structure of the more mobile fraction of pheomelanin was also obtained by means of the analysis of 2D ^{1}H–^{13}C INEPT experiments. Our view is that not only structural features inherent in the pure pigment, but also the role of the matrix structure in defining the overall melanin supramolecular arrangement and the resulting dynamic behavior of the two melanin compounds should be taken into account to explain their functions. The reported results could pave a new way toward the explanation of the molecular origin of the differences in the photoprotection activity displayed by black and red melanin pigments.

Keywords: melanin compounds · molecular dynamics · natural products · NMR spectroscopy · solid-state NMR spectroscopy

Introduction

Melanin compounds are a class of pigment ubiquitously found in the animal and plant kingdoms. These compounds are associated with a variety of biological functions, such as photosensitization, photoprotection, metal-ion chelation, camouflage, thermoregulation, free-radical quenching, and pigmentation of the skin, eyes, and hair. In addition, melanin compounds have been observed to act in interesting nonbiological functions as insulators, semiconductors, ion-exchange resins, and redox polymers.[1]

Three main types of melanin exist in the human body, known as eumelanin (black), pheomelanin (reddish brown), and neuromelanin. The first two classes of melanin are produced within the melanocytes through a biochemical process known as melanogenesis.[2] Even though these two melanins are obtained by starting from a common precursor (i.e., tyrosine), cysteine is involved during the synthesis of pheomelanin.[3] In general, melanosomes produce mixtures of these pigments, with some noted exceptions, such as the pure eumelanic melanosomes in black hair and the retinal pigment epithelium of the eye. Additionally, it has been shown that melanosomes extracted from human red hair are predominantly composed of pheomelanin. The biological functions of melanin compounds are often attributed to their unique chemical properties. However, the exact molecular and supramolecular structures of eumelanin and pheomelanin are still not fully understood. In fact, natural melanin com-

[a] Dr. P. Thureau, Dr. A. Thévand, Dr. S. Viel, Dr. G. Mollica
Institut de Chimie Radicalaire, Spectrométries Appliquées à la Chimie Structurale
CNRS, UMR 7273, Aix-Marseille University
13397 Marseille (France)
Fax: (+33)491-28-28-97
E-mail: giulia.mollica@univ-amu.fr

[b] Dr. F. Ziarelli
Fédération des Sciences Chimiques, Spectropole
CNRS, FR1739, Aix-Marseille University
13397 Marseille (France)

[c] Prof. Dr. R. W. Martin
Department of Chemistry
University of California
92697 Irvine, CA (USA)

[d] Prof. Dr. P. J. Farmer
Department of Chemistry and Biochemistry
Baylor University
76706 Waco, TX (USA)

Supporting information for this article is available on the WWW under http://dx.doi.org/10.1002/chem.201200277.

pounds have resisted structural analysis by conventional spectroscopic techniques because of their substantial insolubility, opacity, and amorphous character, which precluded their study through solution-state hydrodynamic, spectroscopic, light-scattering, and crystallographic techniques. Another important deterrent to the investigation of melanin was the difficulty encountered in their extraction from the protein matrix present in the melanosome and melanocyte. For these reasons, efforts have been made to gain insight into the molecular structure of these pigments by using alternative forms of melanin compounds, such as eumelanin extracted from *Sepia officinalis* or fungi (*Cryptococcus neoformans*), degradation products of various melanin compounds,[4] or synthetic melanins.[5] Particular attention has been paid to the characterization of eumelanin, the most widespread type of melanin in animals and plants. Over the last few years, several techniques have been used for the structural study of eumelanin, in a few cases with the support of theoretical calculations.[6] On the basis of a small number of X-ray scattering studies and first-principles quantum-chemical studies, it was suggested that eumelanin subunits are organized into small planar oligomeric sheets (4–8 monomers), which stack to create nanoaggregates.[7] In a recent study, using low-voltage high-resolution TEM, Watt et al. gave the first direct evidence for the existence of eumelanin protomolecules that stack to form onionlike nanostructures with intersheet spacing between 3.7 and 4.0 Å.[8] Although pheomelanin is less widespread in nature, interest in its characterization has grown due to its correlation susceptibility to skin cancer.[9] Extensive studies carried out in the 1980s showed that pheomelanins are highly heterogeneous polymers or mixtures of polymers with backbones that consist mainly of benzothiazole and tetrahydroisoquinoline units.[10] However, pheomelanin compounds lack any well-defined spectral or other physical characteristics, which makes their structural investigation especially challenging. Few techniques have been applied to the structural and functional elucidation of pheomelanin, notably GC-MS,[11] fluorescence,[12] and ultrafast absorption spectroscopy.[13] Solid-state NMR spectroscopy shows great promise in characterizing the structure and dynamics of materials that lack long-range order, but has rarely been used in the study of melanin compounds. A few reports concern the NMR spectroscopic characterization of eumelanin,[6,14] and only one has reported the ^{13}C solid-state NMR spectrum of pheomelanin.[15]

Herein, 1D and 2D solid-state NMR techniques have been utilized to investigate the structure and dynamics of eumelanin and pheomelanin extracted from human black and red hair, respectively, following the procedure described by Novellino et al.[16] It has been shown that this procedure does not alter the pigment structure, thus retaining the morphology of intact melanosomes.[17] This study has the aim of highlighting differences in the actual supramolecular arrangement and mobility of the two forms of melanin, trying to mimic the conditions in vivo. Our results reveal a significantly higher mobility in red pheomelanin and the presence of two dynamically distinguishable melanin fractions in both black eumelanin and red pheomelanin, in agreement with the different morphologies reported for the two types of melanosome. We argue that not only structural features, but also the presence of a different dynamic behavior, may reflect the differences in the photochemical properties of the two melanin compounds and may also suggest a basis for the correlation of pheomelanin content to UV-radiation damage.

Results

1D solid-state NMR spectra: Figure 1 shows the ^{13}C CP/MAS spectra of eumelanin and pheomelanin extracted from black- and red-hair melanosomes acquired at 400 MHz and 1 GHz. For the sake of discussion, the ^{13}C CP/MAS spectra of both melanin compounds can be divided into three regions:[4] 1) The aliphatic region ($\delta = 15$–80 ppm) , which mainly corresponds to proteins (most likely α-keratins[18] and other proteins that constitute the amorphous matrix that embedded eumelanin in the hair melanosomes) that are still associated with melanin after its enzymatic extraction from hair. In particular, the signals in the region $\delta = 45$–60 ppm correspond to backbone carbon atoms, α-carbon atoms, and threonine/serine β-carbon atoms, whereas the intense envelope in the range $\delta = 10$–45 ppm is due to methylene, methyl, and methine side-chain carbon atoms. 2) The aromatic region ($\delta = 110$–160 ppm), which corresponds to both bulk melanin and protein aromatic residues (tyrosine, phenylalanine, tryptophan, and histidine), together with the signal at $\delta = 157$ ppm, which corresponds to both the imine carbon atom (not aromatic) of arginine and the phenolic aromatic carbon atom of tyrosine. 3) The carbonyl region ($\delta =$ 160–180 ppm), which corresponds to backbone carbonyl groups that belong to the peptidic bonds and side-chain carboxyl and amido groups, together with the carbonyl group of the quinone moieties of melanin (typically at about $\delta =$ 170 ppm). As expected, the ^{13}C CP/MAS spectra of both the black- and red-hair melanosomes exhibit signals that belong to the proteinaceous fraction of the subcellular organelle, thus limiting access to site-specific details about the melanin structure. For this reason, our investigation focused on the use of selective solid-state NMR spectroscopic methodologies to reveal possible differences between the protein and melanin domains, especially in terms of molecular mobility. In general, the spectra of black melanin show broader signals with respect to red melanin. This outcome is true for all the peaks in the spectral region that includes the aromatic carbon atoms, to which the majority of melanin signals can be ascribed. The comparison between the spectra obtained at 400 MHz and 1 GHz (Figure 1) does not reveal any significant change in either the black- or red-hair samples, most notably with respect to the line width. This finding suggests that the observed spectral line broadening is due to static disorder, thus confirming the absence of long-range molecular order in both samples. The lower spectral resolution ob-

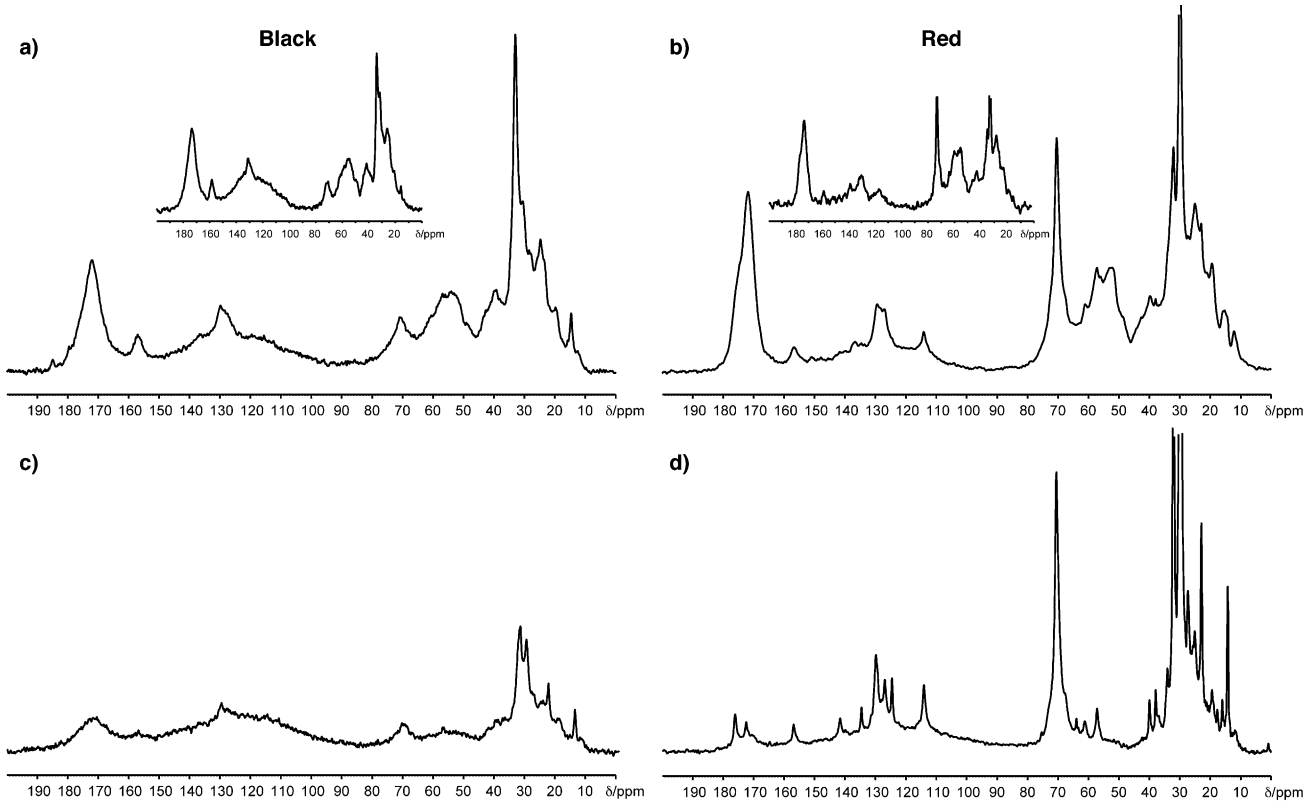

Figure 1. The ^{13}C cross-polarization/magic angle spinning (CP/MAS) spectra of a) black and b) red hair acquired with an external magnetic field of 400 MHz at a spinning rate of 10 kHz. Insets: the corresponding spectra acquired with an external magnetic field of 1 GHz at a spinning rate of 60 kHz are shown for comparison. The ^{13}C direct excitation (DE)/MAS spectra of c) black and d) red hair acquired at 400 MHz with a spinning rate of 10 kHz. The contact times were 1 and 1.5 ms for the black and red hair, respectively. The relaxation delay used in the DE/MAS experiments was 1.5 s.

served for the black-hair sample could be either due to the presence of a larger molecular disorder, a general decreased mobility of the black-hair melanosome components, or both. Paramagnetic effects should also be taken into account, as discussed below. The ^{13}C DE/MAS spectrum of eumelanin (Figure 1c) was acquired by using a short relaxation delay to quench the carbon signals characterized by long spin-lattice relaxation times (^{13}C T_1). This experiment should 1) enhance signals that correspond to carbon atoms richer in protons with respect to less-protonated carbon atoms and 2) quench signals that correspond to nuclei in rigid environments, independently of their proton density. Although quantitative analysis cannot be performed on this spectrum due to the large line width, a comparison with the ^{13}C CP/MAS spectrum shown in Figure 1a reveals a general decrease of the spectral intensity throughout the entire range $\delta = 0$–200 ppm of the ^{13}C NMR chemical shifts. This effect is particularly evident for the regions $\delta = 160$–180, 155–160, and 45–60 ppm, which correspond to the carbonyl, arginine, guanidine (side chain), and protein-backbone carbon atoms, respectively. The only signals that remain clearly visible correspond to some of the protein side-chain β-carbon atoms ($\delta = 10$–40 ppm). Surprisingly, the aromatic signals also remain detectable because only the signal centered at $\delta = 129$ ppm is visibly decreased and the signal at $\delta = 136$ ppm is slightly decreased. Both signals are expected to be mainly due to the melanin protomolecule, which gives a major contribution to this spectral region. On the basis of the structure suggested by Zajac et al.,[19] we do not expect a significantly different mobility for the two aromatic sites (signals at $\delta = 129$ and 136 ppm). On the contrary, different proton densities at the two sites could explain this behavior.[4] However, the possible presence of paramagnetic centers located on quaternary aromatic carbon atoms of melanin should also be taken into account (see below). Figure 1d shows the ^{13}C DE/MAS spectrum of red hair, whereas expansions of the region $\delta = 90$–190 ppm of the ^{13}C CP/MAS, DE/MAS, and NQS/MAS spectra of red hair are shown in Figure 2a–c, respectively. Relative to the corresponding experiment for black hair, the CP and DE/MAS spectra of red hair appear to be generally more resolved. Notably, the aromatic region of the CP/MAS spectrum presents four well-resolved peaks at about $\delta = 114$, 127, 129, and 135 ppm. Additionally, the carbonyl peak centered at about $\delta = 172$ ppm results from two overlapping signals at slightly different isotropic chemical shifts. Also in this case, the DE/MAS spectrum was acquired by using a short relaxation delay. As observed in the black-hair sample, both the regions $\delta = 45$–60 and 160–180 ppm, which correspond to the protein backbone signals, are barely detectable in the DE spectrum, thus suggesting the presence of very restricted protein-chain motions. Only three small peaks are observed at about $\delta = 57$, 61, and

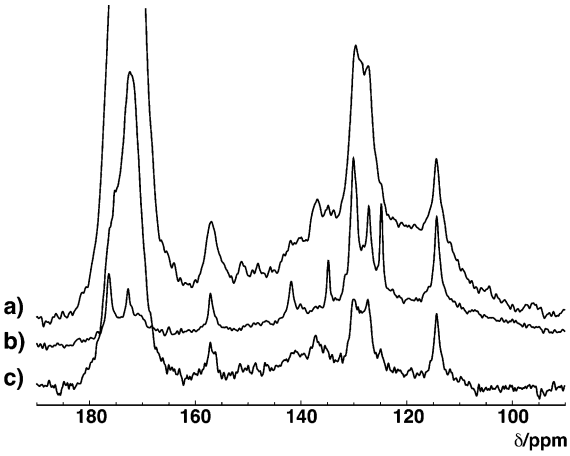

Figure 2. Expansion of the region $\delta = 90$–190 ppm of the a) ^{13}C CP/MAS, b) DE/MAS, and c) nonquaternary suppression (NQS)/MAS spectra of red hair acquired at 400 MHz with a spinning rate of 10 kHz. The contact time and relaxation delay were 1.5 ms and 3 s in the CP and NQS experiments, respectively. A delay of 40 μs was used after cross-polarization in the NQS experiment to allow the dephasing of nonquaternary carbon atoms. The relaxation delay used in the DE/MAS experiments was 1.5 s.

64 ppm, which can be ascribed to the β-carbon atoms of the protein residues, whereas two small peaks are present in the carbonyl region at about $\delta = 172$ and 176 ppm, which can be ascribed to the mobile component of the proteinaceous fraction of the sample (typically, the chain ends). It is very interesting to note the increase in resolution gained in the aromatic region of the DE spectrum of red hair with respect to the CP spectrum. Narrow peaks at about $\delta = 114$, 125, 127, 129, 134, and 142 ppm are clearly visible in the aromatic region, and their intensity in the DE spectrum makes it unlikely that they are exclusively due to the aromatic amino acid residues of the proteinaceous fraction. A dominant contribution from mobile pheomelanin can instead be envisaged. The NQS spectrum of pheomelanin reveals that quaternary carbon atoms contribute significantly to the signals centered at $\delta = 137$–145, 129, 127, and 114 ppm. On the contrary, the signals at $\delta = 125$ and 134 ppm in the DE spectrum are not present in the NQS spectrum, thus indicating that they are due to protonated carbon atoms. It is worth noting that neither of these signals are even visible in the CP spectrum, which could be due to fast dynamics, thus significantly decreasing the heteronuclear dipolar couplings and preventing efficient polarization transfer.

Importantly, the presence of paramagnetic centers located on melanin molecules could, alone, explain the observation of the quaternary aromatic signals (usually characterized by long spin-lattice relaxation times) in the DE spectra of both the black- and red-hair melanosomes. In fact, it is well known that the dipolar coupling of carbon nuclei with unpaired electrons can constitute an efficient relaxation mechanism, thus significantly shortening the spin relaxation times of the involved nuclei. However, this behavior should cause severe line broadening of the peaks in question, which would likely disappear from the spectrum. Moreover, shortening the ^1H $T_{1\rho}$ value would decrease the efficiency of CP transfer toward the carbon atoms that carry—or are near to—the paramagnetic centers. None of these effects is observed in the two samples under consideration. To investigate this aspect, continuous-wave EPR spectra were acquired for both samples, and the obtained spectra (data not shown) were similar to previous EPR spectra acquired on homologous systems.[20] No significant hyperfine coupling was observed and the spectra agreed with the presence of a resonance-stabilized radical (likely in the form of *ortho*-semiquinone and *ortho*-semiquinoneimine for the black and red melanin, respectively). The ratio of the concentration of radical species in the two melanin compounds indicated a tenfold higher concentration of paramagnetic species in the black melanin.

From these observations, we can conclude that the paramagnetic centers are likely to be located at specific sites of the melanin molecules in very low concentration, thus allowing NMR spectroscopic observation of the fraction of melanin protomolecules that do not bear any paramagnetic center. Therefore, the effects observed in the NMR spectra are rather to be ascribed to differences in molecular mobility between the two samples, as discussed in the next section.

2D solid-state NMR spectra: ^1H line-shape analysis: To investigate further the local molecular mobility of eumelanin and pheomelanin, 2D ^1H–^{13}C LG-WISE experiments were recorded on the black- and red-hair melanosomes. These 2D experiments selectively yield the ^1H wide-line spectrum of protons adjacent to the ^{13}C nuclei of interest, hereby providing access to site-specific dynamic information. By analyzing the ^1H line width, true indications about molecular mobility can then be obtained because this parameter is directly related to the inverse of T_2, the value of which increases linearly with mobility and is not affected by spin diffusion. Note also that the use of the Lee–Goldburg cross-polarization scheme allows spin diffusion during the CP contact time to be suppressed. Importantly, the EPR results, which showed isotropic spectra for both black- and red-melanin compounds, suggested that the line width of the ^1H signals in both samples are not significantly affected by the presence of paramagnetic centers.

Sample spinning (10 kHz) caused the ^1H line shapes in the indirect dimension to show the characteristic spinning side-band pattern. Therefore, analysis of the ^1H line shape was used to extract information about the molecular mobility of both samples. The experimental and best-fit calculated line shapes obtained for several selected ^{13}C sites on both red- and black-hair melanosomes by using Equations (2) and (3) (see the Experimental Section) are shown in Figure 3. To find the best-fit function, all the curves were analyzed by trying different combinations of S_1 and S_2, namely, S_1, $S_1 + S_1'$ (i.e., two separate Gaussian distributions of spinning side bands that contribute to the line shape) and $S_1 + S_2$. In our initial guess, only one population (in the form of S_1) contributed to the sample. However, this hypothesis proved not to be good because the central most-intense

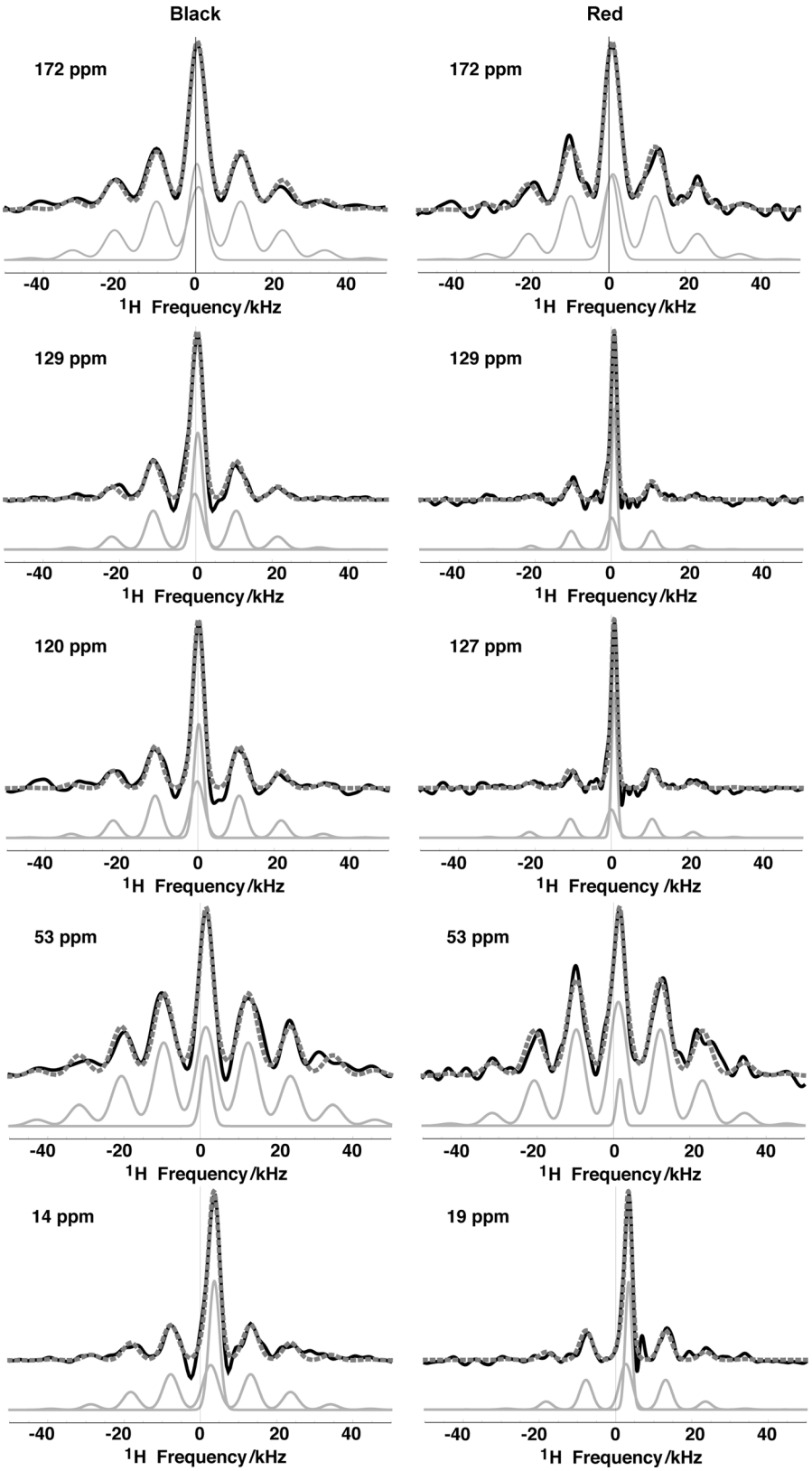

Figure 3. The experimental and best-fit calculated ^{1}H line shapes extracted from the 2D ^{1}H–^{13}C Lee–Goldburg wide-line separation (LG-WISE) experiments performed on black (left) and red (right) hair. The top to bottom curves correspond to $\delta = 172$, 129, 120, 53, and 14 ppm ^{1}H line shapes for black hair and to $\delta = 172$, 129, 127, 53, and 19 ppm ^{1}H line shapes for red hair. Solid gray, dashed gray, and solid black curves indicate the individual best-fit components S_1 (broad) and S_2 (narrow), their sum, and the experimental data, respectively.

peak was underestimated in all cases, whereas the $+1$ and -1 side bands were overestimated. An example of this effect is shown in Figure 4a for the line shape at $\delta = 172$ ppm in the black-hair melanosomes.

Clearly, there was the need for an additional function, which could be another Gaussian distribution of spinning side bands (S_1') or a simple Gaussian function (S_2). The goodness of the fit by using the S_1+S_1' and S_1+S_2 models was quantified by using the adjusted correlation coefficient (R^2) value obtained as an output of the fitting procedure within Mathematica (Wolfram, USA). In both cases, the obtained adjusted R^2 values were significantly larger than those obtained for the single function model, thus indicating an improved match. Moreover, R^2 was consistently slightly higher by using the S_1+S_1' model than by using the function S_1+S_2. However, the improvements in the match by using the S_1+S_1' model were not significant enough to justify the use of such a more complex function, which would require a larger number of parameters to be optimized by the fitting procedure (see Figure 4b,c as an example). Therefore, all the line shapes considered in the analysis were fitted by using the function $S = S_1+S_2$. The ^{13}C NMR chemical shifts were chosen to sample the ^{13}C NMR melanosomes spectra in all the aliphatic (both the protein side-chain and backbone carbon atoms), aromatic, and carbonyl/carboxylic regions. The results of the line-shape analysis show the presence of a broader (S_1) and a narrower (S_2) contribution to the line shapes in both black- and red-hair melanosomes (Figure 5a–c). This outcome indicates that both samples are characterized by two fractions with different mobili-

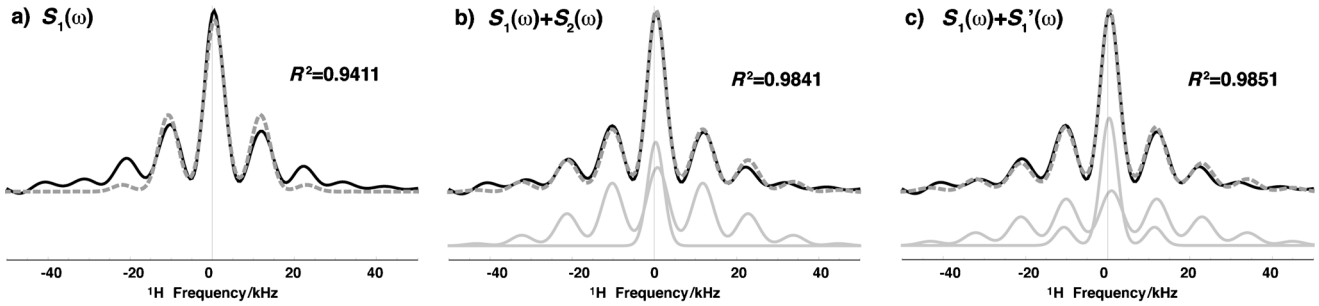

Figure 4. The best-fit results obtained on the line shape for $\delta = 172$ ppm in black hair by using the fit functions: a) S_1, b) $S_1 + S_2$, and c) $S_1 + S_1'$. Solid gray, dashed gray, and solid black curves indicate the individual best-fit components S_1 (broad) and S_2 (narrow), their sum, and the experimental data, respectively. The value of the adjusted correlation coefficients R^2through the different fitting procedures (shown above each plot) allows quantitative evaluation of the fit quality.

ties, namely, S_1 and S_2, which correspond to the rigid and mobile fractions, respectively.

Figure 5a shows the ratio between these two components (S_2/S_1), calculated according to Equation (1):

$$\frac{S_2}{S_1} = \frac{I_2 \cdot \Delta_2}{I_1 \cdot \Delta_1} \quad (1)$$

This quantity gives an indication about the mobile-to-rigid component ratio in the two samples. For all the analyzed proton line shapes, the S_2/S_1 values were lower than ≈ 0.26 and ≈ 0.44 in the black- and red-hair melanosomes, respectively, thus indicating that both samples are mainly rigid. In general, the trend of the S_2/S_1 data within the ^{13}C NMR chemical shifts is similar for the two samples. However, the S_2/S_1 values were generally higher for the red sample (the aromatic and backbone carbon atoms are indicated with gray and light-gray bars, respectively; Figure 5), thus suggesting that the red sample is characterized by a higher amount of the mobile phase with respect to the black sample. The aliphatic signals (light-gray bars, right side; Figure 5) show comparable S_2/S_1 values in the red and black hair. An exception is observed for the carbonyl/carboxyl signals (black bars; Figure 5), thus showing a lower amount of the mobile fraction in the red-hair melanosomes with respect to the black-hair melanosomes. As expected, the ^{1}H line shapes that correspond to the carbonyl groups and protein backbone ($\delta = 172$ and 45–65 ppm, respectively) are characterized by the lowest S_2/S_1 values in both samples, whereas the line shapes that correspond to the aliphatic side-chain carbon atoms of the proteins show the highest fraction of mobile phase in black melanin and the second highest in red melanin. However, quite unexpectedly, the aromatic protons show the highest amount of the mobile fraction in red melanin and the second highest in black melanin. This finding is especially surprising in black melanin, in which the supposed presence of condensed aromatic carbon atoms would instead suggest the presence of a very rigid structure.

Figure 5b,c shows the distribution widths Δ_1 and Δ_2 obtained for the S_1 and S_2 line shapes, respectively. These quantities give an indication about the relative mobility of the two domains present in the black- and red-hair melanosomes. Except for the line shapes that correspond to aromatic protons, which show the lowest values in both samples, all the Δ_1 values vary between 37.0 and 48.6 kHz in the black-hair melanosomes and between 26.4 and 36.5 kHz in the red-hair melanosomes, thus denoting a generally lower mobility of the rigid component in the black sample. In both samples, the aromatic line shapes show the smallest line width, thus suggesting that within the rigid component the melanin molecule, which gives an important contribution to this signal, shows a remarkable mobility with respect to the other sites of the sample. Likewise, the highest Δ_2 values for a given ^{13}C NMR chemical shift are obtained for the signals of the black-hair melanosome, thus indicating that the softer component of eumelanin is still more rigid than the corresponding component in pheomelanin. This effect is more pronounced for Δ_2 than for Δ_1. The only exception is observed for the carbonyl/carboxyl signals, which show decreased dynamics in the red-hair melanosomes with respect to the corresponding signals in the black-hair melanosomes. In both the Δ_1 and Δ_2 analyses, the aromatic carbon atoms exhibit increased mobility relative to the peptidyl and side-chain carbon atoms, which is a clear indication that melanin is characterized by the presence of fast molecular movements in both the red- and black-hair melanosomes, with pheomelanin being less dynamically restrained than eumelanin in both the fractions.

2D solid-state NMR spectra: ^{1}H–^{13}C 2D INEPT of red-hair melanosomes: The ^{1}H–^{13}C 2D INEPT spectrum of red-hair melanosomes acquired by using a magnetic field of 1 GHz and a spinning rate of 60 kHz is shown in Figure 6. INEPT experiments are typically applied to liquid samples, for which signal enhancement can be obtained by exploiting the magnetization transfer between high- and low-γ nuclei (i.e., ^{1}H and ^{13}C, respectively) through the help of scalar coupling (J). The correlation peaks in Figure 6a correspond to ^1J-coupled ^{1}H–^{13}C nuclei; thus, no quaternary carbon atoms are visible in the spectrum. The heteronuclear dipolar decoupling field and relaxation delay used (28 kHz and 1 s, respectively) ensure that only contributions from the more-mobile fraction of the sample, for which the heteronuclear dipolar interaction is already averaged out, are visible in the spec-

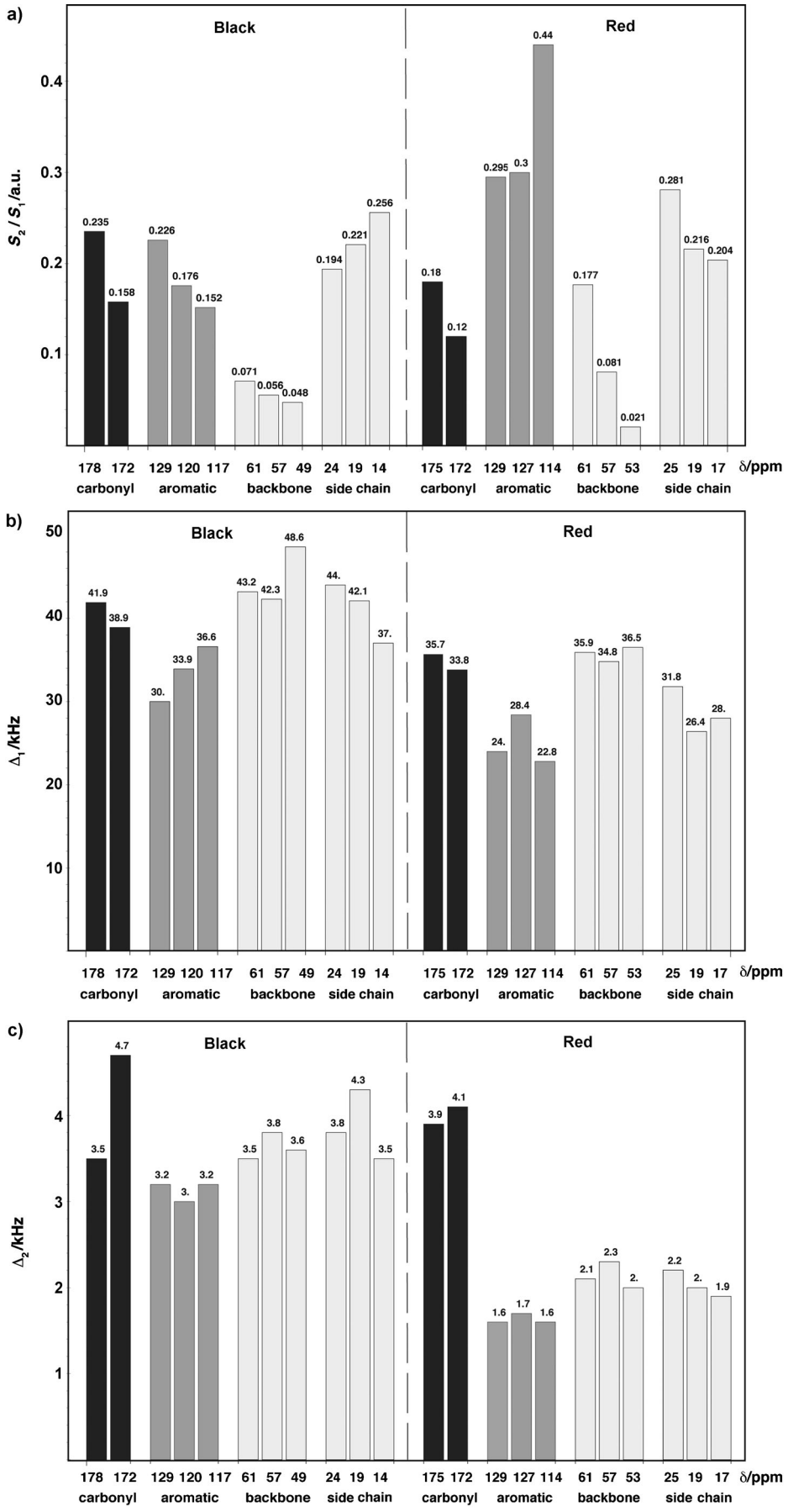

trum. This behavior is confirmed by the absence of signals that belong to the (rigid) protein backbone ($\delta = 45$–60 ppm in the direct dimension), whereas a very crowded area that corresponds to the (more mobile) side chains of the protein residues is visible ($\delta = 15$–45 ppm in the direct dimension). The aromatic region shows the presence of four distinct correlation peaks, which, on the basis of the previous discussion, can be assigned to the more-mobile fraction of red melanin. Because the exact molecular structure of red melanin is unknown, unambiguous assignment of these peaks is not currently possible. However, a tentative assignment can be proposed on the basis of a recent study reported by Greco et al.,[21] in which liquid-state NMR showed, for the first time, that dihydroisoquinoline derivatives constitute key building blocks in the biosynthetic pathway that leads to red-hair pheomelanin (pheomelanogenesis). The tentative assignment is shown in Figure 6b, in which one of the possible chemical structures proposed for the dihydroisoquinoline derivative is also reported. Small chemical-shift differences (of the order of $\Delta\delta = \pm 0.6$ and ± 12 ppm in the ^{1}H and ^{13}C dimensions, respectively) exist between the peaks observed in the 2D INEPT map

Figure 5. Histograms of the values of the a) $S_2/S_1 = (I_2\Delta_2)/(I_1\Delta_1)$ ratio and line widths b) Δ_1 and c) Δ_2 obtained from the best-fit analysis of the ^{1}H line shapes extracted from the ^{1}H–^{13}C 2D LG-WISE experiment on red and black hair. At least two line shapes were analyzed for each of the relevant spectral regions that correspond to carbonyl (black bars), aromatic (gray bars), and aliphatic nuclei (both backbone and side-chain protons of the proteinaceous fraction of the sample; light-gray bars). The shown values (ppm) refer to the chemical shifts of the carbon atoms that correspond to the extracted ^{1}H slice.

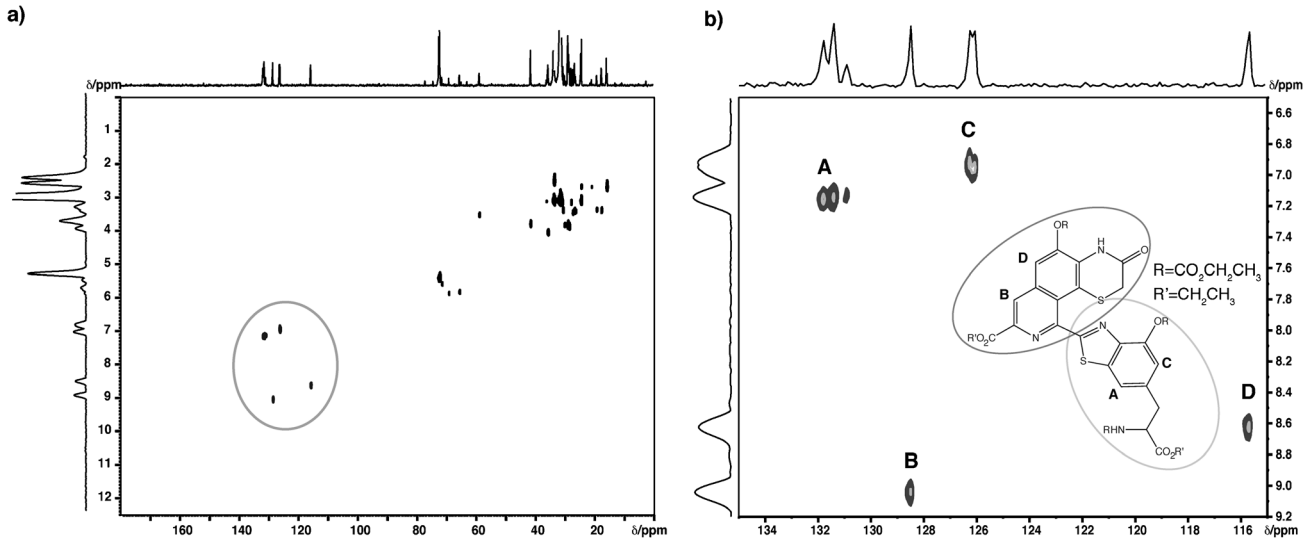

Figure 6. a) The ^{1}H–^{13}C 2D insensitive nuclei enhanced by polarization transfer (INEPT) spectrum of the mobile fraction of red-hair melanosomes acquired with an external magnetic field of 1 GHz and spinning the sample at 60 kHz. The recycle delay was 1 s. Expansion of the region of (a) is indicated with a circle (b). The inset shows the molecular structure of the pheomelanin building block reported by Greco et al.[21] and the tentative assignment discussed in the text.

of red melanin and those reported for the corresponding liquid-state sample (see Table S3 in the Supporting Information).[21] However, considering that the observed chemical-shift values account for the presence of intermolecular effects, both the differences and values remain reasonable. These results are clear evidence of the correct assignment of the aromatic signals to melanin. The molecular structure of the proposed red-melanin building block features a dimeric structure, with two rigid moieties of different dimensions (cyclic structures) connected through a single bond. Deeper inspection of the 2D signals indicated as A and C in Figure 6b reveals the presence of two correlation peaks at very similar ^{1}H and ^{13}C frequencies. Because peaks A and C have been assigned to the benzothiazole moiety of the molecule, the 2D INEPT spectrum suggests that this moiety experiences two different environments, which probably correspond to two distinct supramolecular modes. In future work, this information could be compared with chemical-shift values obtained through first-principles calculations for a series of modified structures.[22] The mobile aromatic protons detected through the INEPT experiment can be considered to coincide with the mobile fraction (S_2) of the red-hair melanosome aromatic protons corresponding to the mobile fraction of pheomelanin. Such protons constitute about 25% of the entire melanosome aromatic protons. The same value can be estimated for black-hair melanosomes to be lower than 20%.

Discussion

It has been shown that the enzymatic treatment used to obtain the samples investigated in the present study preserves the original structure of melanosomes,[16,17] the specialized intracellular organelles in which melanin pigments are synthesized and stored (Figure 7).[3] Although the exact biogenetic path that leads to the formation of melanosomes is still a topic of active research, four major stages have been identified: 1) the synthesis of the tyrosinase enzyme (integrally associated with melanosome membranes); 2) the enlargement of tyrosinase-rich, membrane-limiting vesicles, which, at least in eumelanosomes, acquire a characteristic patterned internal structure probably due to the release of a polypeptide that can generate proteinaceous fibrous striations (unmelanized melanosome or pre-melanosome);[23] 3) activation of tyrosinase and increased the deposition of melanin within the melanosomes along the fibrils until 4) the melanosomes are filled with melanin (mature melanosomes). As the melanin deposition continues, the membranous supports become so obliterated that the granules are devoid of any structural detail.[24] On the basis of this succession of events, we suggest that the two dynamically distinguishable melanin fractions detected can be assigned to: 1) the fraction of melanin that is first deposited onto the fibrillar matrix (S_1 component) and tightly interacts with the fibrils; 2) the fraction of melanin that is deposited later on during the formation of melanosome, less dynamically constrained by the presence of the matrix (S_2 component; in red-hair melanosomes, it is most likely coincident with the mobile fraction selected through DE and INEPT experiments).[25]

It has been reported that melanosome morphology can be significantly affected by various physiological stimuli.[26] Notably, the inhibition of the melanocortin-1 (MC1) G-protein-coupled receptor can make melanocytes switch from the eumelanogenic to pheomelanogenic mode. Essentially, this behavior means that the expression of all the melanosomal proteins is decreased to basal levels and tyrosinase is only

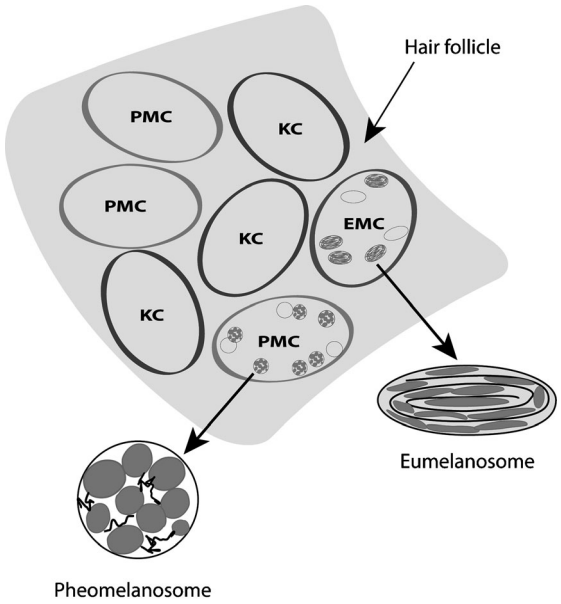

Figure 7. The scheme of the structure of hair follicles showing the presence of pheomelanocytes (PMC), eumelanocytes (EMC), and keratinocytes (KC). Pheomelanosomes and eumelanosomes, the intracellular organelles in which the pigment is synthetized and stored, are also sketched. Pheomelanosomes are spherical and contain an irregular preoteinaceous material (shown as black random chains inside the pheomelanosome) as well as spotty and granular melanin deposits (shown in gray). Eumelanosomes present a more regular proteinaceous fibrillar matrix (sketched as a black solid line inside the eumelanosomes) along which melanin (in gray) is deposited.

expressed at very low levels. Under these conditions, the formation of the fibril matrix that constitutes the physical substrate onto which melanin polymerizes is precluded, and only irregular spotty pheomelanin deposits are obtained on a vesiculoglobular matrix (depicted in Figure 7). This effect could explain the S_2/S_1 values obtained for the two pigments. In fact, the presence of an extended, regular fibrillar matrix in the eumelanosomes can provide a larger number of structural and dynamic constraints, thus increasing the fraction of rigid eumelanin and decreasing the S_2/S_1 values. On the contrary, the lack of a rigid matrix in pheomelanosomes agrees with a larger amount of the mobile fraction (hence, larger S_2/S_1 values). In regard to the results obtained for Δ_1 data, this outcome could explain the higher mobility of the S_1 component (gray bars in Figure 5b) observed in pheomelanin with respect to eumelanin. On the one hand, in black-hair melanosomes, the eumelanin and the protein backbone show comparable S_1 dynamics, thus confirming that this component corresponds to the eumelanin fraction that interacts with the fibrillar matrix of the melanosome. On the other hand, the Δ_1 data collected on the red-hair melanosomes reveal that both pheomelanin and the associated protein are characterized by a significantly larger mobility, in agreement with the hypothesized vesiculoglobular matrix structure. In regard to the results obtained for the Δ_2 data, we can suggest that the more external melanin molecules deposited within the melanosome are less constrained by the interactions with the protein matrix, which is especially true for pheomelanin molecules that possess a less-rigid vesicular matrix. On the basis of these results, we could draw the following picture of the internal organization of black- and red-hair melanosomes. Melanin that belongs to the S_1 component has a decreased mobility in both samples due to the physical hindrance caused by the proximity of the proteinaceous fraction of the melanosome. This effect is more pronounced for eumelanin, which interacts with a fibrillar matrix[23] significantly more rigid and organized than for pheomelanin. In both samples, the mobility observed for melanin and the protein backbone, which is the most representative of the protein-chain dynamics, appears slightly distinct in the S_1 component, with the backbone dynamics always being slightly slower than melanin dynamics. Despite proving the presence of a physical interaction between the two components, no clear evidence of a chemical cross link between melanin and the protein can be inferred from these results. As far as the S_2 component is concerned, both the backbone and side-chain groups in the proteinaceous fraction show very similar dynamics, which can be associated with the protein-chain ends. Also in this case, melanin mobility is higher than that displayed by the corresponding proteinaceous fraction in both the red- and black-hair melanosomes. This behaviour is compatible with the fact that melanin that belongs to the S_2 component is somehow far from the protein core, possibly only slightly interacting with the chain ends, but generally keeping a marked degree of dynamic freedom.

In addition to the above considerations about the mobility of the melanin environment in black- and red-hair melanosomes, we argue that the chemical structure of the black- and red-melanin protomolecules should also play an important role in determining the mobility of this more external layer. The hypothesis of the presence of condensed aromatic rings in black melanin is in agreement with a decreased mobility with respect to red melanin, for which a less-reticulated network should be expected on the basis of its hypothetical molecular structure. Instead, the presence of side-chain alanyl and/or cysteinyl residues is expected to contribute to the decreased dynamics observed for the carbonyl/carboxyl signals in red-hair melanosomes with respect to black-hair melanosomes concerning the mobile S_2 component. In fact, hydrogen bonds involving the carboxyl group of these residues are expected to stabilize the network of red-melanin protomolecules in the form of 3-oxo-3,4-dihydro-1,4-benzothiazine, benzothiazole, trichochrome C, or pyridine-2,3,4,6-tetracarboxylic acid and 2-(4,5-dicarboxythiazol-2-yl)-3,4,6-pyridine tricarboxylic acid units.[21]

Conclusion

Melanin constitutes the key component of the human pigmentary system. For a long time it has resisted characterization by conventional spectroscopic techniques due to its inherent physicochemical properties. Such properties not only

define the function of melanin, but are also strongly related to its molecular and supramolecular architecture in the melanosome. A better understanding of melanin structural features at a molecular or cellular level would then lead to a better comprehension of its macroscopically observable properties and functions. This study has shown that solid-state NMR spectroscopy can be successfully used for the investigation of the structural and dynamic behavior of natural melanin pigments extracted from human hair. Notably, the combination of 1D and 2D experiments has revealed the presence of two dynamically distinct components in both melanin forms and a distinctly higher mobility in red melanin. Site-specific information about the mobility of the two components was obtained through the quantitative analysis of the ^{1}H line shapes extracted from ^{1}H–^{13}C 2D LG-WISE spectra. We argue that a different morphology of the proteinaceous matrix that comprises the internal structure of the eu- and pheomelanosomes could be at the origin of the significantly distinct overall mobility of the black and red pigment. In eumelanosomes, the presence of an extended more-rigid fibrillar matrix generates physical constraints that decrease molecular movements. On the contrary, the deposition of pheomelanin occurs in mainly vesiculoglobular melanosomes, in the absence of a proper proteinaceous matrix. This explanation agrees well with the faster overall mobility of red melanin and with the observation of a higher mobile-to-rigid phase ratio in red hair. These peculiar properties allow the mobile fraction of red melanin to behave, from an NMR point of view, as a liquidlike sample. This effect allowed further structural investigation of this fraction by using 1D selective and 2D INEPT experiments. A tentative assignment of the different peaks visible for this fraction was also possible, which agrees with recently reported data from the biomimetic oxidation of the pheomelanin precursor 5-*S*-cysteinyldopa. Such detailed spectral insight will be usable in the future for comparison with first-principle calculations of chemical shifts for suggested structures. In a recently reported review[27] that presents the latest results on the characterization of black and red melanin, Simon and Peles reported a quote from Hearing: "*Melanosomes provide a unique and rich environment for research, with many significant and diverse implications for human health*".[28] The results presented herein demonstrate that new insight into deeper understanding of the actual role and function of eumelanin and pheomelanin can be gained by taking into account not only the characteristics of the pure/isolated pigment, but also its environment in vivo. The knowledge of the overall architecture of the pigment in the melanosome, which also includes the proteinaceous matrix, should not be separated from its dynamic behavior. By considering the structural and dynamic aspects together, new ways for a better comprehension of the differences in the optical properties of black and red melanin could be paved.

Experimental Section

Materials: Proteinase K, papainase, proteinase type XVI, and Trinton X-100 were purchased from Sigma–Aldrich. Dithiothreitol was purchased from EMD Chemicals. A package of black Remy hair was purchased from European Hair Extensions (CA, USA). A sample of red hair was obtained from an anonymous donor. High-purity argon and nitrogen gas were used. The reaction cells used were either a three-neck 1000 mL round-bottomed flask with a gas inlet and outlet (either high-purity argon or nitrogen) to a bubbler flask filled with water or a titration cell with a capacity of 500 mL, also equipped with a gas inlet and outlet to a bubbler flask.

Melanin extraction procedures: A sample of black hair was with acetone (2×), dichloromethane (1×), and diethyl ether (1×) to remove the sebum and allowed to air dry overnight. The washed hair was subsequently cut into pieces of 2 mm. A sample of cut black hair (23 g) was added to a three-neck 1000 mL round-bottomed flask under a N_2 head-gas purge. Enough phosphate buffer (0.1 M, pH 7.4) was added to submerge all the hair, and the reaction mixture was maintained at 370 °C with a thermostat and sonicated for 30 min. Dithiothreitol (3 g) was added to the reaction mixture, which was sonicated for 30 min and allowed react overnight with slow stirring. The next day, proteinase K (250 mg) and dithiothreitol (1.45 g) were added to the reaction mixture, which was sonicated for 30 min and allowed to react overnight with slow stirring. On day 3, a pellet was generated by centrifugation of the solution, the supernatant was discarded, and the pellet was washed with nanopure water (3×). The pellet was resuspended in phosphate buffer for digestion with papain (100 mg) and dithiothreitol (500 mg). On day 4, a pellet was generated again from the solution, the supernantant was discarded, and the pellet was washed with nanopure water (3×) and resuspended in phosphate buffer with the addition of protease XIV (100 mg) and dithiothreitol (200 mg). On day 5, a pellet was generated again from the solution, resuspended in deareated phosphate buffer, and Trinton X-100 (0.4 mL) was added. The solution was allowed to stir for 4 h. A pellet was generated again from the sample, the supernantant was discarded, and the pellet was washed with nanopure water (4×) and resuspended in deareated buffer with protease XIV (100 mg) and dithiothreitol (250 mg) for overnight digestion with slow stirring. On day 6, a pellet was generated from the sample, washed with nanopure water (3×), resuspended in a small amount of water, frozen in dry ice, and lyophilized to obtain eumelanin (453 mg), which was stored in a desiccator. An analogous method was used to extract pheomelanin from the red-hair sample with twice the amount of hair utilized, while the amount of enzymes used was kept constant. The reaction mixture was not stirred with a magnetic bar, but shaken at 95 rpm in a thermostated shaker.

Solid-state NMR methods 400 MHz: Solid-state NMR spectroscopic experiments were performed using a 9.4 Tesla external magnet (i.e., 400 and 101 MHz for the ^{1}H and ^{13}C resonances, respectively) and a Bruker Avance III spectrometer equipped with a ^{1}H–X CP/MAS probe for 4 mm rotors with a spinning speed of 10 kHz. The data were acquired at room temperature. All the experiments were performed with a recycle delay of between 3 and 4 s (to allow for the recovery of ^{1}H magnetization), except for the ^{13}C DE experiments, which were performed with a recycle delay of 1.5 s on both the black- and red-hair samples. The ^{13}C CP/MAS experiments were performed with contact times of 40–1000 μs for the black hair and 1500 for red hair; about 10000 scans were acquired in all the cases. The ^{13}C NQS experiments[29] were performed with the same parameters used in the CP experiments, except that a delay of 40 μs without ^{1}H decoupling was introduced before acquisition. During the CP-like experiments, the ^{1}H radio-frequency (RF) field used for the excitation pulse of 90° was 80 kHz. During contact time, an RF field of 40 kHz was used on the ^{13}C channel, whereas a linear-ramped RF amplitude with an average field strength of 50 kHz was used on the ^{1}H channel to broaden the Hartmann–Hahn matching profile. In all the experiments, the two-pulse phase modulation (TPPM) decoupling scheme[30] was applied using a RF field of 80 kHz. The ^{1}H–^{13}C 2D wide-line separation (WISE) experiment was acquired using Lee–Goldburg cross polarization (LG-CP) to quench spin diffusion during the CP contact time.[31] In this case, a linear ramp with

an average RF field strength of 45 kHz was used on the ^{13}C channel, whereas no ramp was used on the ^{1}H channel to avoid mismatching from the Hartmann–Hahn Lee–Goldburg conditions. For both samples, 128 rows, each acquired with 1024 scans, were collected. TPPM heteronuclear decoupling was used in the direct dimension to get isotropic ^{13}C spectra.

1 GHz: High-resolution solid-state experiments on black- and red-hair melanin were performed using a static magnetic field of 23.5 Tesla (i.e., 1 GHz and 250 MHz for the ^{1}H and ^{13}C resonances, respectively), which was made available by the CRMN facility in Lyon (http://www.ens-lyon.fr/crmn), on a Bruker Avance III console. In all the cases, the sample was packed into a rotor with a diameter of 1.3 mm and spun at 60 kHz using a triple-channel CP/MAS probe. The temperature was set to 245 K to compensate for frictional heating (effective temperature: 293 K). On this spectrometer, ^{1}H–^{13}C CP/MAS spectra were acquired using 70000 and 80000 scans on both the black- and red-hair samples. RF fields of 13 and 47 kHz were applied on the ^{1}H and ^{13}C channels, respectively, during the contact time. A swept-frequency TPPM[32] heteronuclear decoupling scheme was applied during the ^{13}C acquisition. This spectrometer was also used to acquire the ^{1}H–^{13}C 2D refocused insensitive nuclei enhanced by polarization transfer (INEPT)[33] spectrum on the red-hair melanin sample. In this experiment, globally optimized alternating-phase rectangular pulses (GARP)[34] broadband decoupling with a RF field of 28 kHz was applied during the acquisition, whereas no homonuclear decoupling was used during t_1. Two echo delays were used in the sequence. The first echo delay was set at 1.9 ms (corresponding to the theoretical value $1/(4\times{}^{1}J)$, where ${}^{1}J = 130$ Hz), whereas the second echo delay was set at 1.3 ms, which guaranteed that all CH, CH_2, and CH_3 signals had a positive sign. The CP contact time in this experiment was set at 1 ms. A total of 320 scans were acquired in the direct dimension for each of the 399 rows with a relaxation delay of 1 s.

Analysis of LG-WISE experiments: To extract information about the mobility of the black and red melanin in the two samples, a quantitative analysis of the ^{1}H line shapes extracted from the 2D ^{1}H–^{13}C LG WISE spectra was performed.[35] In all the cases, the ^{1}H line shapes were fitted by using a combination of equations ((2) and(3)) previously described by Emsley and co-workers[36] and recently used by Kumashiro and co-workers to study the mobility of elastin:[37]

$$S_1(\omega) = \sum_{i=-n}^{n} I_1 \cdot \exp\left\{-4\ln 2 \cdot \left[\left(\frac{n\omega_r}{\Delta_1}\right)^2 + \left(\frac{\omega - \omega_{01} - n\omega_r}{\lambda_1}\right)^2\right]\right\} \quad (2)$$

$$S_2(\omega) = I_2 \cdot \exp\left\{-4\ln 2 \cdot \left(\frac{\omega - \omega_{02}}{\Delta_2}\right)^2\right\} \quad (3)$$

In the present analysis, $S_1(\omega)$ and $S_2(\omega)$ (elsewhere indicated as S_1 and S_2, respectively, for the sake of simplicity) indicate the broader and narrower line-shape contributions, with respective intensities I_1 and I_2, central frequencies ω_{01} and ω_{02}, and widths Δ_1 and Δ_2; λ_1 indicates the width of each spinning side band; and ω_r is the spinning frequency. Therefore, the S_1 contribution is a Gaussian distribution of spinning side bands, whereas S_2 is a simple Gaussian function without any spinning side-band distribution. For the purposes of our analysis, n was chosen equal to 4 to take into account four spinning side bands on each side of the line-shape envelope. The nonlinear fitting of the experimental ^{1}H line shapes was performed using the NonlinearModelFit function embedded in Mathematica 8.0 (Wolfram, USA).

Acknowledgements

Financial support from the TGIR RMN THC Fr3050 for conducting part of the research is kindly acknowledged. G.M., F.Z., and P.T. thank Dr. Moreno Lelli, Dr. Anne Lesage, and Dr. Bénédicte Elena for their support during the experiments performed at the CRMN facility in Lyon and for helpful discussions. G.M., F.Z., P.T., and S.V. thank Dr. Béatrice Tuccio for support with the EPR data. G.M. acknowledges support of the European Commission under a Marie Curie IntraEuropean Fellowship (grant number IEF-FP7-PEOPLE2008–237339). R.W.M. acknowledges support from NSF CAREER CHE-0847375.

[1] M. d'Ischia, A. Napolitano, A. Pezzella, P. Meredith, T. Sarna, *Angew. Chem.* **2009**, *121*, 3972–3979; *Angew. Chem. Int. Ed.* **2009**, *48*, 3914–3921.
[2] S. Ito, *Pigm. Cell Res.* **2003**, *16*, 230–236.
[3] K. Jimbow, O. Ishida, S. Ito, Y. Hori, C. J. Witkop, R. A. King, *J. Invest. Dermatol.* **1983**, *81*, 506–511.
[4] a) S. Ghiani, S. Baroni, D. Burgio, G. Digilio, M. Fukuhara, P. Martino, K. Monda, C. Nervi, A. Kiyomine, S. Aime, *Magn. Reson. Chem.* **2008**, *46*, 471–479; b) B. B. Adhyaru, N. G. Akhmedov, A. R. Katritzky, C. R. Bowers, *Magn. Reson. Chem.* **2003**, *41*, 466–474.
[5] a) P. Reinheimer, J. Hirschinger, P. Granger, P. Breton, A. Lagrange, P. Gilard, M. A. Lefebvre, N. Goetz, *Biochim. Biophys. Acta Gen. Subj.* **1999**, *1472*, 240–249; b) M. Hervé, J. Hirschinger, P. Granger, P. Gilard, A. Deflandre, N. Goetz, *Biochim. Biophys. Acta* **1994**, *1204*, 19–27.
[6] K. B. Stark, J. M. Gallas, G. W. Zajac, J. T. Golab, S. Gidanian, T. McIntire, P. J. Farmer, *J. Phys. Chem. B* **2005**, *109*, 1970–1977.
[7] K. C. Littrell, J. M. Gallas, G. W. Zajac, P. Thiyagarajan, *Photochem. Photobiol.* **2003**, *77*, 115–120.
[8] A. A. R. Watt, J. P. Bothma, P. Meredith, *Soft Matter* **2009**, *5*, 3754–3760.
[9] a) E. Wenczl, G. P. Van Der Schans, L. Roza, R. M. Kolb, A. J. Timmerman, N. P. Smit, S. Pavel, A. A. Schothorst, *J. Invest. Dermatol.* **1998**, *111*, 678–682; b) M. R. Vincensi, M. d'Ischia, A. Napolitano, E. M. Procaccini, G. Riccio, G. Monfrecola, P. Santoianni, G. Prota, *Melanoma Res.* **1998**, *8*, 53–58.
[10] a) R. B. Deibel, M. R. Chedekel, *J. Am. Chem. Soc.* **1982**, *104*, 7306–7309; b) R. M. B. Deibel, M. R. Chedekel, *J. Am. Chem. Soc.* **1984**, *106*, 5884–5888.
[11] D. N. Dernroth, A. Rundström, B. Kagedal, D. Nezirević Dernroth, A. Rundström, B. Kågedal, *J. Chromatogr. A* **2009**, *1216*, 5730–5739.
[12] S. P. Nighswander-Rempel, *Biopolymers* **2006**, *82*, 631–637.
[13] T. Ye, J. D. Simon, *J. Phys. Chem. B* **2003**, *107*, 11240–11244.
[14] a) H. Knicker, G. Almendros, F. J. González-Vila, H.-D. Lüdemann, F. Martin, *Org. Geochem.* **1995**, *23*, 1023–1028; b) G. A. Duff, J. E. Roberts, N. Foster, *Biochemistry* **1988**, *27*, 7112–7116; c) S. Aime, M. Fasano, B. Bergamasco, L. Lopiano, G. Quattrocolo, *Adv. Neurol.* **1996**, *69*, 263–270; d) S. Tian, J. Garcia-Rivera, B. Yan, A. Casadevall, R. E. Stark, *Biochemistry* **2003**, *42*, 8105–8109; e) J. Zhong, S. Frases, H. Wang, A. Casadevall, R. E. Stark, *Biochemistry* **2008**, *47*, 4701–4710.
[15] Y. Liu, L. Hong, K. Wakamatsu, S. Ito, B. Adhyaru, C.-Y. C.-Y. Cheng, C. R. Bowers, J. D. Simon, *Photochem. Photobiol.* **2005**, *81*, 135–144.
[16] L. Novellino, A. Napolitano, G. Prota, *Biochim. Biophys. Acta Gen. Subj.* **2000**, *1475*, 295–306.
[17] Y. Liu, V. R. Kempf, J. B. Nofsinger, E. E. Weinert, M. Rudnicki, K. Wakamatsu, S. Ito, J. D. Simon, *Pigment Cell Res.* **2003**, *16*, 355–365.
[18] J. Yu, D. W. Yu, D. M. Checkla, I. M. Freedberg, A. P. Bertolino, *J. Invest. Dermatol.* **1993**, *101*, 56S-59S.
[19] G. W. Zajac, J. M. Gallas, J. Cheng, M. Eisner, S. C. Moss, A. E. Alvarado-Swaisgood, *Biochim. Biophys. Acta Gen. Subj.* **1994**, *1199*, 271–278.
[20] a) R. C. Sealy, C. C. Felix, J. S. Hyde, H. M. Swartz, *Free Radicals Biol.* **1980**, *4*; b) M. S. Blois, B. Zahlan, J. E. Maling, *Biophys. J.* **1964**, *4*, 471–490; c) R. C. Sealy, J. S. Hyde, C. C. Felix, I. A. Menon, G. Prota, H. M. Swartz, S. Persad, H. F. Haberman, *Proc. Natl. Acad. Sci. USA* **1982**, *79*, 2885–2889.
[21] G. Greco, L. Panzella, L. Verotta, M. d'Ischia, A. Napolitano, *J. Nat. Prod.* **2011**, *74*, 675–682.
[22] A. L. Webber, S. Masiero, S. Pieraccini, J. C. Burley, A. S. Tatton, D. Iuga, T. N. Pham, G. P. Spada, S. P. Brown, *J. Am. Chem. Soc.* **2011**, *133*, 19777–19795.

[23] a) J. F. Berson, A. C. Theos, D. C. Harper, D. Tenza, G. Raposo, M. S. Marks, *J. Cell Biol.* **2003**, *161*, 521–533; b) I. Hurbain, W. J. C. Geerts, T. Boudier, S. Marco, A. J. Verkleij, M. S. Marks, G. Raposo, *Proc. Natl. Acad. Sci. USA* **2008**, *105*, 19726–19731; c) B. Watt, G. van Niel, D. M. Fowler, I. Hurbain, K. C. Luk, S. E. Stayrook, M. A. Lemmon, G. Raposo, J. Shorter, J. W. Kelly, M. S. Marks, *J. Biol. Chem.* **2009**, *284*, 35543–35555.
[24] K. Hall, L. J. Wolfram, *J. Soc. Cosmet. Chem.* **1975**, *26*, 247–254.
[25] R. P. R. Dawber, D. A. Fenton, in *Diseases of Hair and Scalp*, 3rd ed., Blackwell Science, Oxford, **1997**, pp. 397–417.
[26] a) T. Kushimoto, J. C. Valencia, G.-E. Costin, K. Toyofuku, H. Watabe, K.-I. Yasumoto, F. Rouzaud, W. D. Vieira, V. J. Hearing, *Pigm. Cell Res.* **2003**, *16*, 237–244; b) A. Slominski, J. Wortsman, P. M. Plonka, K. U. Schallreuter, R. Paus, D. J. Tobin, *J. Invest. Dermatol.* **2005**, *124*, 13–21.
[27] J. D. Simon, D. N. Peles, *Acc. Chem. Res.* **2010**, *43*, 1452–1460.
[28] V. J. Hearing, *Pigm. Cell Res.* **2000**, *13 Suppl 8*, 23–34.
[29] S. J. Opella, M. H. Frey, *J. Am. Chem. Soc.* **1979**, *101*, 5854–5856.
[30] A. E. Bennett, C. M. Rienstra, M. Auger, K. V. Lakshmi, R. G. Griffin, *J. Chem. Phys.* **1995**, *103*, 6951.
[31] a) B. J. Van Rossum, C. P. De Groot, V. Ladizhansky, S. Vega, H. J. M. De Groot, *J. Am. Chem. Soc.* **2000**, *122*, 3465–3472; b) V. Ladizhansky, S. Vega, *J. Chem. Phys.* **2000**, *112*, 7158.
[32] a) R. S. Thakur, N. D. Kurur, P. K. Madhu, *Chem. Phys. Lett.* **2006**, *426*, 459–463; b) C. Vinod Chandran, P. K. Madhu, N. D. Kurur, T. Bräuniger, *Magn. Reson. Chem.* **2008**, *46*, 943–947.
[33] a) G. A. Morris, R. Freeman, *J. Am. Chem. Soc.* **1979**, *101*, 760–762; b) B. Elena, A. Lesage, S. Steuernagel, A. Böckmann, L. Emsley, *J. Am. Chem. Soc.* **2005**, *127*, 17296–17302; c) T. Kern, M. Giffard, S. Hediger, A. Amoroso, C. Giustini, N. K. Bui, B. Joris, C. Bougault, W. Vollmer, J.-P. Simorre, *J. Am. Chem. Soc.* **2010**, *132*, 10911–10919.
[34] A. J. Shaka, J. Keeler, *Prog. Nucl. Magn. Reson. Spectrosc.* **1987**, *19*, 47–129.
[35] a) N. Zumbulyadis, *Phys. Rev. B* **1986**, *33*, 6495–6496; b) K. Schmidt-Rohr, J. Clauss, H. W. Spiess, *Macromolecules* **1992**, *25*, 3273–3277.
[36] S. Hediger, A. Lesage, L. Emsley, *Macromolecules* **2002**, *35*, 5078–5084.
[37] K. Ohgo, W. P. Niemczura, T. Muroi, A. K. Onizuka, K. K. Kumashiro, *Macromolecules* **2009**, *42*, 8899–8906.

Received: January 25, 2012
Published online: July 12, 2012

